

RESEARCH LETTER

10.1002/2016GL072371

Key Points:

- Bio-Argo float data elucidate biogeochemical dynamics in a productive anticyclonic ocean eddy in the South Indian Ocean subtropical gyre
- Stirring of the deep chlorophyll maximum by anticyclonic eddy-induced mixing leads to enhanced surface chlorophyll
- Advection of productive waters can also enhance surface chlorophyll in anticyclonic eddies

Supporting Information:

- Supporting Information S1

Correspondence to:

F. Dufois,
francois.dufois@uwa.edu.au

Citation:

Dufois, F., N. J. Hardman-Mountford, M. Fernandes, B. Wojtasiewicz, D. Shenoy, D. Slawinski, M. Gauns, J. Greenwood, and R. Toresen (2017), Observational insights into chlorophyll distributions of subtropical South Indian Ocean eddies, *Geophys. Res. Lett.*, *44*, 3255–3264, doi:10.1002/2016GL072371.







Received 19 DEC 2016

Accepted 22 MAR 2017

Accepted article online 23 MAR 2017

Published online 9 APR 2017

Observational insights into chlorophyll distributions of subtropical South Indian Ocean eddies

François Dufois^{1,2} , Nick J. Hardman-Mountford¹ , Michelle Fernandes³ ,
Bozena Wojtasiewicz¹ , Damodar Shenoy³, Dirk Slawinski¹ , Mangesh Gauns³ ,
Jim Greenwood¹, and Reidar Toresen⁴

¹CSIRO Oceans and Atmosphere, Indian Ocean Marine Research Centre, Crawley, Western Australia, Australia, ²ARC Centre of Excellence for Coral Reef Studies, The UWA Oceans Institute, Crawley, Western Australia, Australia, ³National Institute of Oceanography, CSIR, Goa, India, ⁴Institute of Marine Research, Bergen, Norway

Abstract The South Indian Ocean subtropical gyre has been described as a unique environment where anticyclonic ocean eddies highlight enhanced surface chlorophyll in winter. The processes responsible for this chlorophyll increase in anticyclones have remained elusive, primarily because previous studies investigating this unusual behavior were mostly based on satellite data, which only views the ocean surface. Here we present in situ data from an oceanographic voyage focusing on the mesoscale variability of biogeochemical variables across the subtropical gyre. During this voyage an autonomous biogeochemical profiling float transected an anticyclonic eddy, recording its physical and biological state over a period of 6 weeks. We show that several processes might be responsible for the eddy/chlorophyll relationship, including horizontal advection of productive waters and deeper convective mixing in anticyclonic eddies. While a deep chlorophyll maximum is present in the subtropical Indian Ocean outside anticyclonic eddies, mixing reaches deeper in anticyclonic eddy cores, resulting in increased surface chlorophyll due to the stirring of the deep chlorophyll maximum and possibly resulting in new production from nitrate injection below the deep chlorophyll maximum.

1. Introduction

Mesoscale eddies are common features of oceanic circulation [Chelton *et al.*, 2011b] and play an important role in enhancing biological production [e.g., Klein and Lapeyre, 2009; McGillicuddy *et al.*, 1998]. Established in the 1990s, the “eddy-pumping” mechanism describes an upwelling of nutrient-rich subsurface water into the euphotic zone that enhances biological productivity in cyclonic eddies (CEs) [Falkowski *et al.*, 1991]. Although the eddy-pumping idea is still popular [e.g., Stramma *et al.*, 2013], recent literature demonstrates that eddies can impact biogeochemical cycles through a range of processes [Chelton *et al.*, 2011a; Gaube *et al.*, 2014; McGillicuddy, 2016; McGillicuddy *et al.*, 2007], including some which are also likely to enhance productivity in anticyclonic eddies (ACEs) [Dufois *et al.*, 2014, 2016; McGillicuddy *et al.*, 2007].

The South Indian Ocean subtropical gyre has been described as unique in this respect because surface chlorophyll (Chl) is enhanced in ACEs compared to CEs during winter [Dufois *et al.*, 2014; Gaube *et al.*, 2013]. It has been shown that in fact all five subtropical gyre areas exhibit an eddy response similar (although weaker) to the South Indian Ocean [Dufois *et al.*, 2016], suggesting that the eddy-pumping mechanism is less dominant than previously thought. Several competing processes have been suggested to increase primary production in the South Indian Ocean ACEs, including eddy-induced Ekman pumping [Gaube *et al.*, 2013] and eddy-induced mixing [Dufois *et al.*, 2014, 2016], but the balance of the processes involved is still the subject of ongoing debate [McGillicuddy, 2016]. In oligotrophic environments the main Chl signal is often located out of view of satellites, within the deep chlorophyll maximum (DCM) [Huisman *et al.*, 2006]. However, most previous studies relied on satellite surface Chl, lacking the vertical resolution necessary to fully characterize the eddy-induced Chl response.

Here we use in situ data from a recent austral-winter cruise across the South Indian Ocean subtropical gyre to describe the physical-biological interactions at the mesoscale in the region. We show for the first time how eddy-induced mixing interacts with the DCM and discuss previous results in light of our findings.

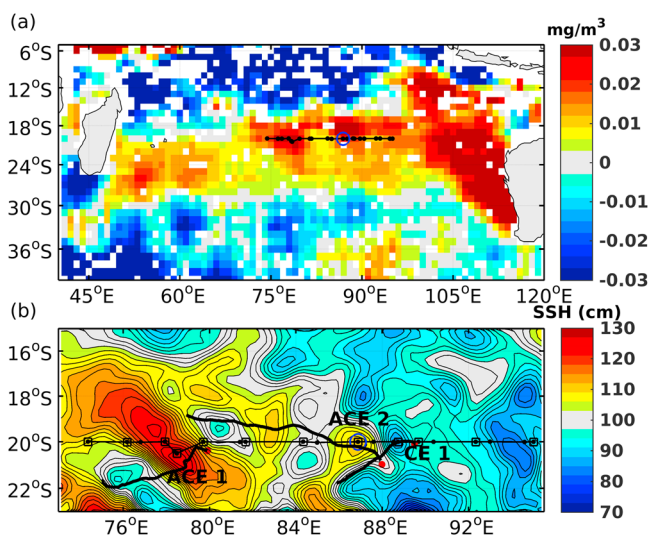


Figure 1. Position of the CTD casts (black dots) and deployment of the Bio-Argo float (blue circle). (a) The background map, adapted from *Dufois et al.* [2014], corresponds to the difference between surface Chl in ACEs and CEs in winter (June–August). (b) SSH (cm) on the 06 July 2015. SSH contours are every 2 cm. The black squares indicate stations where water sampling was carried out. The locations of the three eddies referred to as ACE 1, ACE 2, and CE 1 are indicated. The tracks of those eddies over their entire lifespan are also indicated by the black lines, with the red dots corresponding to the location of first detection.

together with underway fluorescence. Discrete measurements of nitrate, Chl *a*, phaeopigment, and dissolved oxygen from Niskin bottles on the CTD rosette were undertaken and used to calibrate the CTD-mounted sensors (see the supporting information).

2.2. Bio-Argo Float

A biogeochemical profiling float (NAVIS, Sea-Bird Scientific Inc.), hereafter referred to as Bio-Argo, was deployed in the center of an ACE on 5 July 2015 (Figure 1). This Bio-Argo measured conductivity, temperature, and depth; dissolved oxygen; fluorescence; and optical backscattering at two different wavelengths (see the supporting information). In this study, we present 2 months of data acquired by the float after the deployment (the float itself was still operational at the time of writing: 18 February 2017). The CTD-rosette cast conducted at the time of deployment was used to calibrate the oxygen and fluorescence sensors, and the particulate backscattering coefficient b_{bp} [Boss and Pegau, 2001] for the two wavelengths (see the supporting information). We also computed the particulate backscatter slope γ as an indicator of the particle size distribution, with the slope decreasing for larger particles, according to *Antoine et al.* [2011] (see the supporting information).

2.3. Other Data

We derived several variables from the CTD and Bio-Argo vertical profiles. The mixed layer depth (MLD) was computed following *de Boyer Montégut et al.* [2004] by using a criterion on potential density changes (see the supporting information). The vertical diffusivity K_z is derived from the *Thorpe* [1977] scale following *Park et al.* [2014] (see the supporting information).

We used satellite Chl from Moderate Resolution Imaging Spectroradiometer Aqua (MODIS) (<http://oceancolor.gsfc.nasa.gov>) at 4 km resolution, sea surface height (SSH) and geostrophic velocities from Archiving, Validation, and Interpretation of Satellite Oceanographic data (AVISO) (<http://www.aviso.oceanobs.com/>) at 0.25° resolution, and surface net heat fluxes from National Centers for Environmental Prediction (NCEP)/National Center for Atmospheric Research [Kalnay et al., 1996] at ~1.9° resolution. Those products were collocated in time and space along the cruise track.

2. Methods and Data

2.1. EAF-Nansen Project Voyage Across the Southern Indian Ocean

We undertook a 21 day research voyage (26 June to 16 July 2015) from Jakarta (Indonesia) to Port Louis (Mauritius) to investigate oceanographic and ecological features in the region as part of the EAF-Nansen Project of the Food and Agriculture Organization of the United Nations. In this study, we present data from a total of 21 stations sampled within 8 days (03–10 July 2015) located along a longitudinal transect around 20°S in the center of the basin (Table S1 in the supporting information), corresponding to a region where ACEs exhibit higher winter surface Chl (Figure 1). Continuous profile data from conductivity-temperature-depth (CTD), fluorometer, multispectral backscattering meter and dissolved oxygen sensors were recorded,

2.4. Eddy and Water Mass Tracking

Using the daily SSH field, the eddies encountered during the cruise were followed by using the eddy tracking algorithm developed by *Halo et al.* [2014]. Several eddy parameters were computed (see the supporting information), including the position and the radius R of the core. We calculated the distance r from the float to the eddy center and normalized it by the eddy radius (r/R). We also located the eddy edges by using the outermost SSH closed contour around the eddy location.

We also ran particle tracking experiments to track the eddy water masses origin [*Feng et al.*, 2010, 2016]. Particles were seeded regularly every 0.01° of latitude and longitude inside the outermost eddy SSH closed contour and passively advected backward in time by using the daily AVISO geostrophic velocities. To assess the origin of the water masses encountered along the cruise track, we also used oxygen, salinity, and nitrate from the World Ocean Circulation Experiment hydrographic section I08°N along 80°E [*Schlitzer*, 2000; *Talley and Baringer*, 1997].

3. Results

3.1. Eddies Sampled During the Cruise

Three eddy cores were encountered along the cruise track: a CE (referred to as CE 1) near 89°E and two ACEs, one near 78.5°E (referred to as ACE 1) and the other at 87°E (referred to as ACE 2) (Figures 1b and 2a). CE 1 was the smallest eddy with an average core radius of 56 km around the time of sampling, while ACE 1 and ACE 2 had a radius of 74 and 72 km, respectively (Table S2). Further, their radii stayed fairly constant over their entire life. The three eddies appeared relatively “young”; the eddy tracking tool first detected CE 1, ACE 1, and ACE 2 at 19, 22, and 27 days, respectively, before the time of the CTD-cast (Table S2). CE 1 was the earliest to disappear after the cruise, with a total lifespan of 70 days, while ACE 1 and ACE 2 lasted for 117 and 132 days, respectively. They all had a mostly westward propagation (Figure 1 and Table S2) and were all generated between 20 and 21°S . Further, the three eddies appeared to be nonlinear because their rotational speed is far greater than their propagation speed [*Chelton et al.*, 2011b].

3.2. Along-Track Data

Downward sloping isopycnals below the MLD were noticeable in both ACEs, while upward sloping isopycnals could be seen in the CE (Figure 2c). Surface Chl from the underway measurement and SSH were positively correlated ($r=0.48$, $p<0.05$) along the cruise track. The MLD and the SSH were also correlated ($r=0.66$, $p<0.05$ after spatially detrending both variables). Accordingly, the two ACE cores coincided with deeper MLD (61 and 131 m for ACE 1 and ACE 2, respectively) and higher surface Chl (0.24 and 0.18 mg m^{-3}) compared to CE 1 (MLD was 40 m, and Chl was 0.11 mg m^{-3}) (Figure 2a). Active vertical mixing was seen in the core of both ACE 1 and ACE 2 over the mixed layer (mean K_z was 0.048 and $0.039\text{ m}^2\text{ s}^{-1}$, respectively), with higher vertical diffusivity than in surrounding waters (Figure 2g). Potential density inversions were observed in the mixed layer of both ACEs (in Figure 2g the potential density profile is stable only where Thorpe-derived vertical diffusivities are undefined). The potential density profile of CE 1 was stable throughout the water column.

Within the mixed layer Chl values were higher in the core of ACE 1 and ACE 2 (0.14 and 0.12 mg m^{-3} over the mixed layer) than within CE 1 (0.05 mg m^{-3}) (Figure 2f). The phaeopigment fraction was also increased in the ACEs compared to the CE within the mixed layer (Figures S3c and S3d). A DCM was present at every station along the voyage track (Figure 2f); however, it showed variability both in terms of depth (mean value of 110 m, ranging from 85 to 153 m) and amplitude (mean value of 0.65 mg m^{-3} , ranging from 0.36 to 0.88 mg m^{-3}). In both ACEs the DCM was located immediately below the MLD (Figure 2f) (It is important to note that this was not evidenced when looking at water bottle samples (Figure S3b in the supporting information); we believe that the DCM peak has been missed during the discrete sampling procedure). In ACE 1 the DCM was shallower (85 m) than in the surrounding waters, with comparable average Chl concentration (0.68 mg m^{-3}). In ACE 2, which exhibited the deepest MLD, the DCM was also the deepest (153 m) and the weakest (0.36 mg m^{-3}) observed along the track. While depth-integrated (0–150 m) Chl and phaeopigment concentrations were slightly higher in the vicinity of ACE 1, they were lower in ACE 2 than in the surrounding waters (Figure S3e; those results should, however, be regarded with care due to the discrete nature of the water bottle sampling). A low-oxygen layer at around 200 m depth was observed across the section

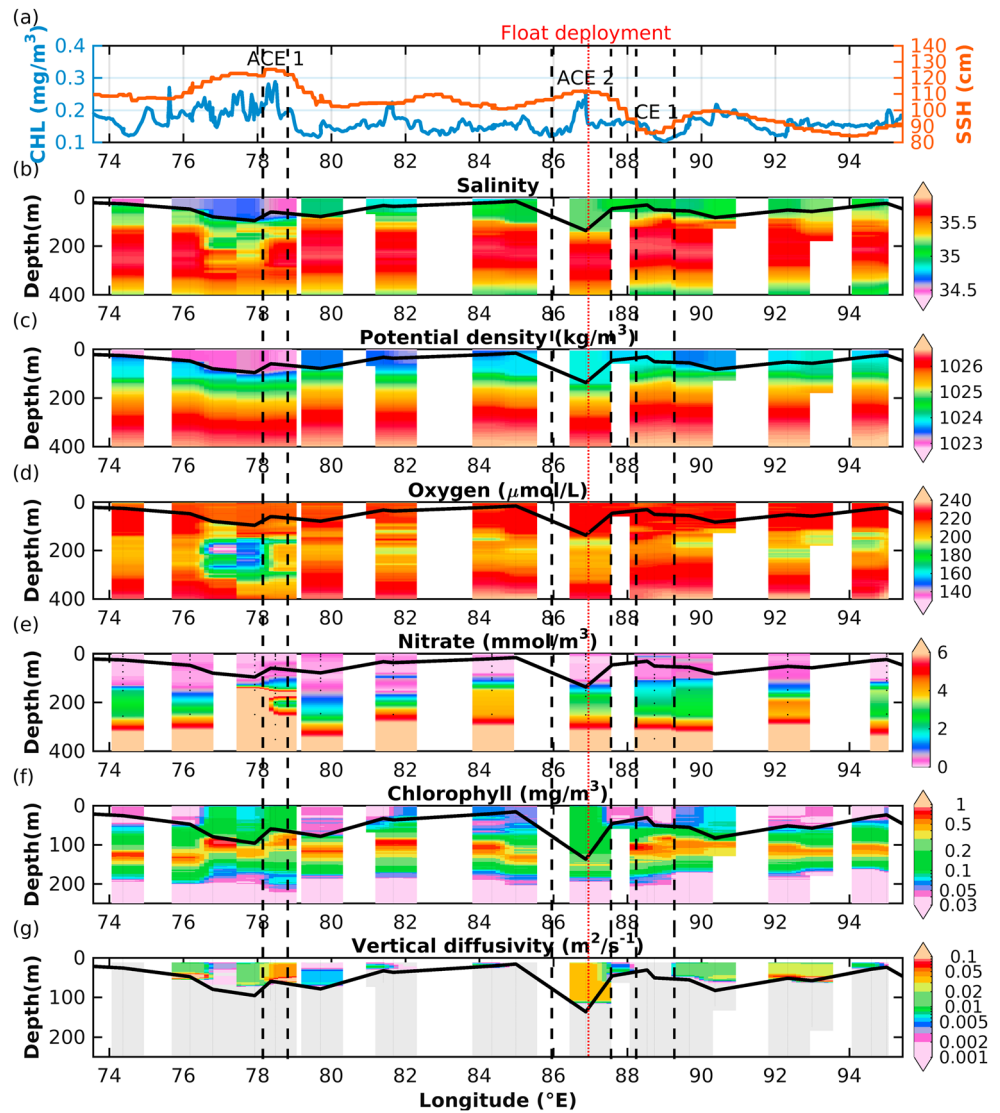


Figure 2. Transect along 20°S. (a) Chl (mg m^{-3}) from the shipboard thermosalinograph and SSH along the cruise track from altimetry. (b and c) Salinity and potential density (kg m^{-3}) from the onboard CTD. (d) Dissolved oxygen ($\mu\text{mol/L}$) from the CTD-mounted sensor. (e) Nitrate (mmol m^{-3}) from water samples. (f) Chl (mg m^{-3}) from the CTD-mounted fluorescence sensor from 0 to 250 m. (g) Vertical diffusivity ($\text{m}^2 \text{s}^{-1}$) derived from the Thorpe scale from 0 to 250 m; the grey shading denotes regions where vertical diffusivity cannot be defined (no potential density inversions were found). The location of the CTD casts are indicated on Figure 1. The MLD is marked as the black line (Figures 2b–2g). The red dashed line indicates the float deployment station. The location of three eddies is indicated in the first panel. The two crossings of the cruise track with the outermost SSH closed contour for each of the three eddies is indicated by the vertical black dashed lines.

(Figure 2d). This oxygen minimum was strongly enhanced westward of ACE 1 ($129 \mu\text{mol L}^{-1}$ versus $186 \mu\text{mol L}^{-1}$ on average across the section) and, to a lesser extent, in ACE 1 core ($163 \mu\text{mol/L}$). Lower salinity and a shallower nitracline were also observed in the vicinity of ACE 1 (Figures 2b, 2e, and S4). In the eastern ACE 2, the nitracline is slightly deeper and the mixed layer nitrate concentration smaller than in nearby CE 1 (1 mmol m^{-3} contour found at 145 m and 112 m, respectively) (Figure 2e). Further, ACE 2 was the only location along the section where the nitrate concentration immediately below the MLD reached $\sim 1 \text{ mmol m}^{-3}$.

3.3. Float Data

A Bio-Argo float was deployed close to the center of ACE 2 and followed the eddy for ~ 6 weeks, in a range of ~ 2 eddy radii, before exiting the eddy (Figure 3). Taking the eddy center as the reference point, the float

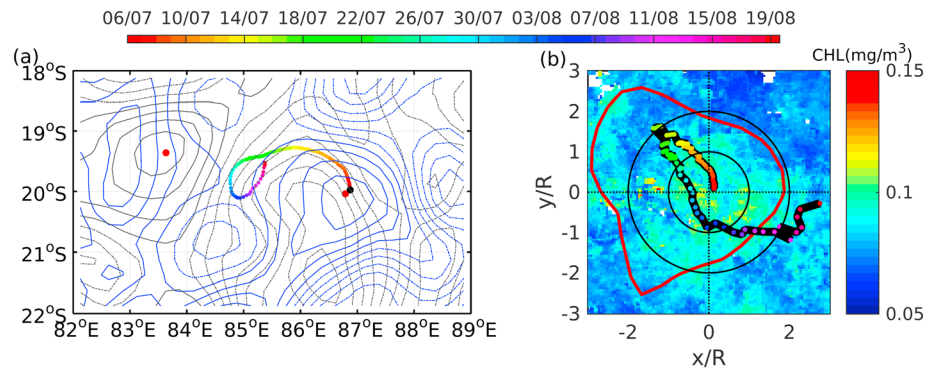


Figure 3. Trajectory of the Bio-Argo float from 5 July 2015 to 20 August 2015. (a) Deployment position on 5 July (black point) and subsequent trajectory (colored line with corresponding dates) of the float. The blue and grey lines correspond to the contours of SSH (every 2.5 cm, and dashed below 100 cm) from altimetry on the deployment day and on 20 August 2015, respectively. The red dots correspond to the position of ACE 2 center tracked by the float for the same dates. (b) Float trajectory (colored line with corresponding dates) in the eddy frame of reference. The intersection of the dotted lines is the eddy center, and the two circles correspond to 1 and 2 eddy radius, respectively. The color shading corresponds to the satellite Chl (mg m^{-3}) averaged over the same period in the eddy frame of reference. The red contour corresponds to the outermost SSH closed contour of ACE 2 on 14 July.

initially headed toward the north-west edge of the eddy before crossing the eddy in a south-eastward direction (Figure 3b). On 14 July the float was the closest to the eddy edge, but still inside the outermost SSH closed contour of the eddy (Figure 3b). The float exited the outermost SSH closed contour on 12 August. The composite averaged (over 47 days) satellite-derived surface Chl following the eddy frame of reference showed a slight increase of Chl in the eddy core compared to outside the core (0.096 and 0.081 mg m^{-3} on average for $r \leq R$ and $R < r < 3R$, respectively) (Figure 3b). During the initial ~ 2 days the float encountered rapid oceanographic changes highlighted by a shallowing of the MLD (Figures 4 and S5). The float started in a region of deep MLD ($\sim 130 \text{ m}$) before entering a region with a shallower MLD ($\sim 30 \text{ m}$) while moving away from the eddy center. From 06 to 11 July, the mixed layer Chl decreased from 0.15 to 0.06 mg m^{-3} , while the DCM concentration increased from 0.35 to 0.54 mg m^{-3} (Figure 4d). Subsequently, from 16 July to 15 August, a roughly symmetrical pattern emerged as the float crossed the eddy through the eddy core (Figures 4 and S4). The MLD was deeper close to the eddy center ($\sim 160 \text{ m}$) and shallower toward both edges (40 to 80 m). Evidence of mixed layer entrainment was seen in the dilution of surface waters by deeper waters, associated with a decrease of the oxygen saturation level and an increase of salinity close to the eddy center (Figure S5). There was also evidence that vertical mixing in the eddy core remained active. Indeed, nonzero vertical diffusivities computed from the Thorpe scale were due to the presence of inversions in the potential density profile whose length scale was consistent with the depth of the mixed layer (Figure 4c).

The MLD deepening toward the eddy center was associated with an increase of the mixed layer Chl (up to 0.15 mg m^{-3} at the beginning of the time series and 0.18 mg m^{-3} around 31 July), while the DCM weakened, eventually vanishing completely (Figure 4d). However, there was no clear trend in terms of depth-integrated Chl at the eddy scale (Figure 4g). Nonetheless, closer to the eddy edge and outside the eddy, there is a clear decoupling between the mixed layer and the DCM in terms of Chl and backscatter, while closer to the eddy center Chl was well-mixed throughout the surface layer (Figures 4d, 4e, and S4f). This was also evident when looking at the particulate backscatter to chlorophyll ratio (Figure 4f), an indicator of phytoplankton photoacclimation state [Behrenfeld and Boss, 2003; Westberry et al., 2010]. Outside the eddy or close to the eddy edge, the DCM exhibited a weaker backscatter to chlorophyll ratio compared to the mixed layer, due to the higher relative contribution of Chl. Closer to the center, the higher relative contribution of Chl in the well-mixed, one-layer system (no DCM layer) also resulted in a weaker backscatter to Chl ratio compared to surrounding mixed layer waters outside the eddy, although stronger than within the surrounding DCM. The backscatter slope (γ) indicated that away from the ACE core, smaller particles predominated above the MLD compared to the DCM. This contrasts with the mixed layer close to the ACE core, in which larger particles are seen compared to the upper mixed layer away from the eddy core (Figure S5g). Both of these indicators suggest that the phytoplankton population within the mixed layer of the eddy was more similar to the DCM population than the

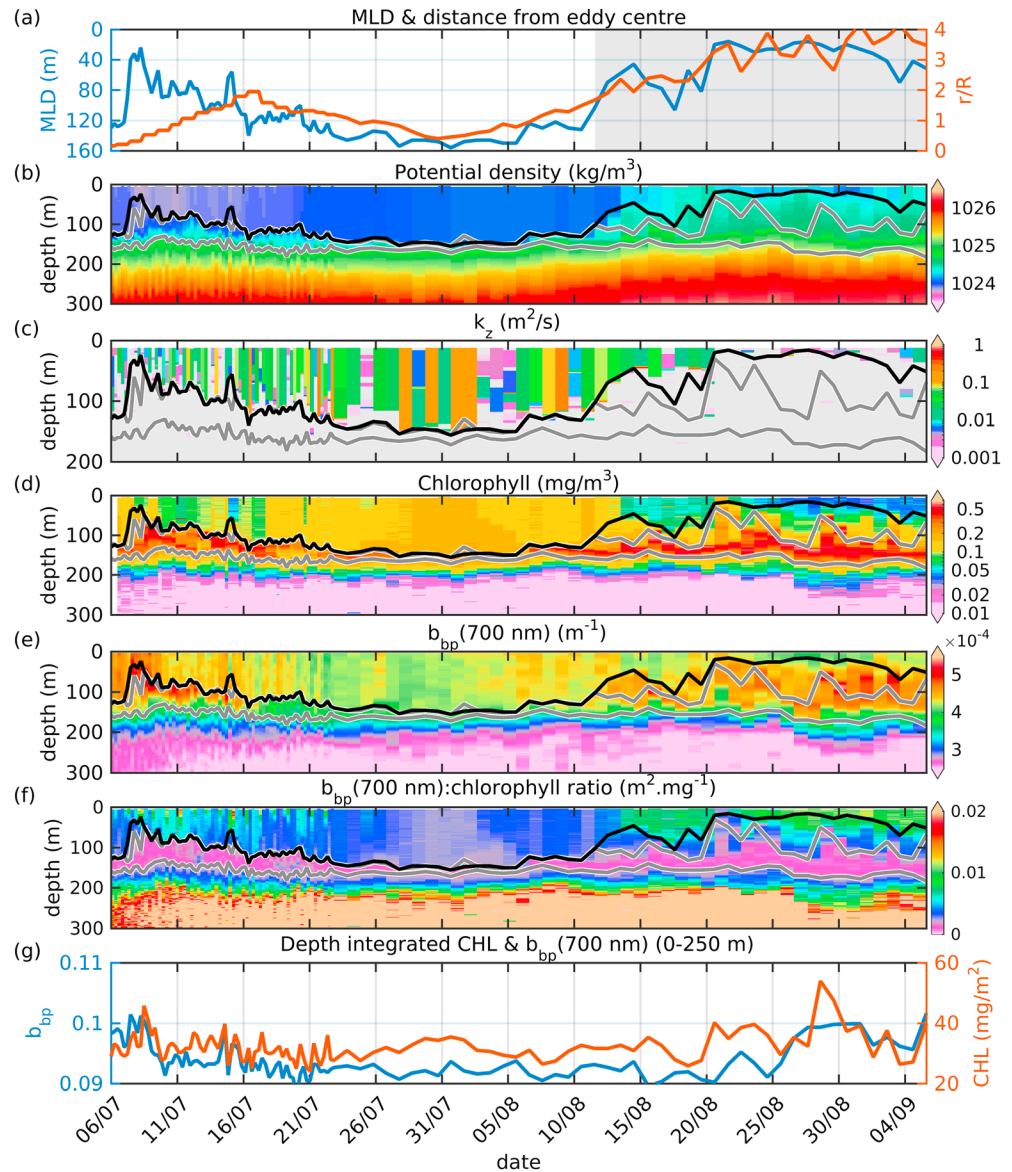


Figure 4. Bio-Argo float data. (a) MLD (m) in blue and distance from the eddy center normalized by eddy radius r/R in red. The grey area corresponds to periods when the float is outside ACE 2 outermost SSH closed contour. (b) Potential density (kg m^{-3}). (c) Vertical diffusivity computed from the Thorpe scale ($\text{m}^2 \text{s}^{-1}$); the grey shading denotes regions where no potential density inversions were found. (d) Chlorophyll (mg m^{-3}). (e) Particulate backscatter at 700 nm (m^{-1}). (f) Particulate backscatter at 700 nm to chlorophyll ratio ($\text{m}^2 \text{kg}^{-1}$). (g) Depth-integrated (from surface to 250 m) Chl (mg m^{-2}) in red and particulate backscatter at 700 nm in blue. The DCM extent (0.3 mg m^{-3} contours) are indicated by the grey lines (Figures 4b–4f). The MLD is marked as the black line (Figures 4b–4f).

surface population outside the eddy. Further, while the first profiling period close to the eddy center (from 05 July) was associated with a depth-integrated backscatter increase, the second period (around 31 July) did not show any trend (Figure 4g). Overall there was an increase in backscatter after 25 August, when the float was well outside the eddy structure and the MLD clearly shallower.

4. Discussion

By combining float data with ship-based measurements, we demonstrate that horizontal advection of productive waters, and deeper vertical mixing in ACEs are two mechanisms able to explain the observed surface Chl increase in ACEs in winter in the South Indian subtropical gyre.

4.1. Advection of Productive Waters

The water masses located directly westward of ACE 1 had a strong oxygen minimum around 200 m, a shallower nitracline, and lower salinity above ~400 m compared to waters along 20°S (Figures 2b, 2d, 2e, and S4). Those anomalies are also observed in ACE 1 core, albeit to a lesser extent. The particle tracking experiments showed that the water masses inside ACE 1 originated 3 months earlier from two main sources located to the north around 69–72°E, 16–18°S and 80–86°E, 12–14°S (Figure S6). The water masses in the northern source regions, if advected southward, would present oxygen, nitrate, and salinity anomalies consistent with those observed around ACE 1 (Figure S7) [Talley and Baringer, 1997]. Therefore, we suggest that the anomalies observed in the vicinity of ACE 1 are driven by horizontal advection of water from the north, rather than by local biogeochemical processes.

Since ACE 1 has been generated along 20°S and propagated westward (Figure 1), the water masses observed at the time of sampling have not been propagated by the eddy itself from the north. However, ACE 1 is part of a larger-scale counterclockwise rotating feature (Figure 1). We suggest that this larger-scale structure has been advecting water from the Indonesian throughflow jet [Talley and Baringer, 1997] southward. Those waters characterized by higher nitrate concentration and depth-integrated Chl eventually ended up in ACE 1. This would explain why oxygen, nitrate, and salinity anomalies are more intense just outside the eddy on its west side. This result is consistent with previous studies which showed that ACEs in the South Indian Ocean preferentially entrain elevated Chl and nutrients from the north [Gaubert et al., 2013, 2014].

4.2. Deeper Mixing

No evidence of productive water intrusion from the north was observed in the easternmost ACE 2 (no water mass anomalies were found at this location (Figure 2)). For this eddy we suggest that deeper winter convective mixing in ACEs [Dufois et al., 2014; Kouketsu et al., 2012] was responsible for the increase of Chl at the surface. Three potentially coexisting mechanisms could result from the deeper winter mixing: (i) the DCM is stirred into the mixed-layer through entrainment, (ii) phytoplankton in the mixed layer have photoacclimated to a reduction in average light available, and (iii) nutrients are injected from below the MLD into the mixed layer, supporting new phytoplankton production.

1. In the DCM, cells are photoacclimated to low light [Dubinsky and Stambler, 2009] and present higher intracellular pigmentation (lower backscatter to Chl ratio) than closer to the surface. In the center of ACE 2, the upper layer was well mixed and also had a lower backscatter to Chl ratio with both elevated Chl and decreased backscatter contributing to the relationship (Figures 4d–4f). Those changes in the mixed layer were consistent with the putative upward transport of low-light acclimated cells from the DCM. Upward mixing of phytoplankton cells from the DCM was also evidenced by the higher phaeopigment concentration and increased phaeopigment to Chl ratio in the mixed layer of ACE 2 (Figure S3d), which is typical of deeper waters including the DCM.
2. Looking only to mixing to explain these observed changes supposes that once the phytoplankton cells are mixed upward they do not have time to reacclimate to their new light environment, a process that operates over a time frame of hours to days, depending on species and a range of environmental factors [Prézelin et al., 1991]. The elevated surface Chl and lower backscatter to Chl ratio at the surface in ACE 2 was observed for over 20 days (Figure 4f); thus, photoacclimation within the mixed layer may also contribute to this relationship over the time frame of the observations. Phytoplankton cells would experience lower light on average than in mixed layer waters outside the eddy as they are mixed deeper through the water column, and therefore increase their intracellular pigmentation [Behrenfeld et al., 2015].
3. The mixed layer penetrated into higher nitrate layers in the core of ACE 2 compared to the surrounding waters (Figure 2e). As such, we expect an increase of nitrate supply into the mixed layer of the ACE and a concomitant increase of phytoplankton biomass. This concept is consistent with previous studies which demonstrated that deeper mixing in ACEs is able to enhance nitrate fluxes to the mixed layer in subtropical gyres increasing surface chlorophyll concentrations [Dufois et al., 2014, 2016]. Thus, the observed increase of fluorescence (Figure 4d) in the ACE core would correspond to an increase of phytoplankton biomass from new production. Chl tends to be added to phytoplankton assemblages through the addition of larger-sized cells [Chisholm, 1992]. Consistently, we observed changes in the spectral slope of backscattering implying that particles in the mixed layer at the center of ACE 2 were larger than surface particles outside the eddy (Figure S5g). It is, however, difficult to solely attribute those changes to a

change of the community structure. Indeed, a pure mixing effect between the larger DCM particles and the smaller surface particles would produce the same result. Furthermore, the reduced backscatter at the surface in the center of ACE 2 (Figure 4e) and the lack of increase in depth-integrated backscatter (Figure 4g) could be seen to indicate that there was no increase in biomass. However, as larger particles backscatter less than smaller particles [Stramski and Kiefer, 1991], we suggest that this signal could be partly due to an increase in particle size within the assemblages rather than a lack of new biomass. The relative backscatter decrease (lower backscatter to Chl ratio) (Figure 4f) could also be due to the injection of clearer (lower backscatter) water from beneath the MLD and the production of a “fresh” phytoplankton bloom with less detritus and heterotrophic activity than an “older” bloom [Lignell *et al.*, 1993; Sorokin, 1977].

Overall, it is difficult to attribute the observed changes in Chl to only one mechanism and it seems likely that mixing, photoacclimation, and new production were all contributing factors.

4.3. Eddy/Chl Variability

Using ocean color remote sensing data, it has been previously shown that Chl is enhanced in ACEs compared to CEes during winter in the South Indian subtropical gyre [Dufois *et al.*, 2014; Gaube *et al.*, 2013] and, to a lesser extent, in the subtropical gyres of other ocean basins [Dufois *et al.*, 2016]. Through shipboard and float data we show for the first time that this relationship holds only within the mixed layer. The eddy response deeper down at the DCM seems to be variable and can even be opposite to the surface/mixed layer response (Figure 4d).

4.4. Temporal Versus Spatial Interpretation

One of the difficulties of analyzing float data is that changes can happen both spatially and temporally. Here we are confident that the variability observed around the eddy is spatial (i.e., related to the eddy structure), rather than temporal, for various reasons. (i) We observed a deepening of the mixed layer toward the ACE center (Figure 4a) consistent with global observations [Dufois *et al.*, 2016]. Deeper winter MLD is an intrinsic characteristic of ACEs due to weaker preexisting stratification compared to surrounding waters [Dufois *et al.*, 2014; Kouketsu *et al.*, 2012]. (ii) The variability highlighted by the Bio-Argo float around the ACE is consistent with that observed at a quasi-synoptic scale along the cruise track. (iii) The deep MLD encountered within ACE 2 stands out from the rest of the time series over the float entire lifespan (Figure S8). The net heat flux could be driving the MLD changes at the seasonal timescale, but not within ACE 2 (Figures S5a and S8). This is consistent with the study of Pookkandy *et al.* [2016] highlighting the importance of ocean dynamics, on top of local forcing, in shaping the mixed layer in the subtropical Indian Ocean.

5. Conclusion

Bio-Argo floats have been used in previous studies to assess the seasonal cycle of phytoplankton biomass in subtropical gyres [Mignot *et al.*, 2014]. For the first time here we have used results from a Bio-Argo float to assess the phytoplankton response to eddies in oligotrophic environments. Measuring multiple properties of the phytoplankton community with an autonomous float has proved valuable in understanding the mechanisms driving observed biogeochemical changes. Combining winter observations from ship and float we have provided evidence for two mechanisms likely to enhance surface Chl in ACEs in the South Indian Ocean subtropical gyre. ACEs can trap productive waters through horizontal advection and/or locally modify the chlorophyll distribution through enhanced convective mixing. The question of whether or not the deeper mixing in ACEs induces nutrient injection and new production, or only a stirring of the DCM, remains unclear, and could be investigated in the future by combining productivity measurements with Bio-Argo float deployments and using a modeling approach similar to that of Chenillat *et al.* [2015].

References

- Antoine, D., D. A. Siegel, T. Kostadinov, S. Maritorena, N. B. Nelson, B. Gentili, V. Vellucci, and N. Guillocheau (2011), Variability in optical particle backscattering in contrasting bio-optical oceanic regimes, *Limnol. Oceanogr.*, *56*(3), 955.
- Behrenfeld, M. J., and E. Boss (2003), The beam attenuation to chlorophyll ratio: An optical index of phytoplankton physiology in the surface ocean?, *Deep Sea Res., Part 1*, *50*(12), 1537–1549.
- Behrenfeld, M. J., R. T. O'Malley, E. S. Boss, T. K. Westberry, J. R. Graff, K. H. Halsey, A. J. Milligan, D. A. Siegel, and M. B. Brown (2015), Reevaluating ocean warming impacts on global phytoplankton, *Nat. Clim. Change*, *6*, 323–330, doi:10.1038/nclimate2838.

Acknowledgments

We thank the NASA Ocean Biology Group (OB.DAAC) for providing the MODIS Aqua Ocean Color Data (<http://oceancolor.gsfc.nasa.gov>) and P. Penven for providing an eddy-tracking tool. NCEP Reanalysis data were provided by the NOAA/OAR/ESRL PSD, Boulder, Colorado, USA (<http://www.esrl.noaa.gov/psd/>). The altimeter products were produced by Ssalto/Duacs and distributed by AVISO, with support from CNES (<http://www.aviso.altimetry.fr/duacs/>). The Bio-Argo data are available on GDAC FTP servers (<http://doi.org/10.17882/42182>) at <ftp://ftp.ifremer.fr/ifremer/argo/dac/csiro/5904924/>. The cruise data can be provided by the Institute of Marine Research, Bergen, Norway. Contact person: Reidar Toresen (reidar@imr.no). We thank the captain, the crew, and the scientific and technical staff on board the R/V “Dr Fridtjof Nansen” for their contribution to the data acquisition. We thank various scientists from IMR, CSIR-NIO, ESSO-INCOIS (Ministry of Earth Sciences), and CSIRO for their support in acquiring quality controlled data. We thank the Argo team of the Integrated Marine Observing System (IMOS) for their technical support. We acknowledge funding from the Australian Government through the Australia-India Strategic Research Fund (AISRF). Funding support for the Indian side was provided by the Department of Science and Technology. We thank Hema Naik and Pooja Satardekar for their analytical help. F.D. was supported through a CSIRO OCE Postdoctoral Fellowship.

- Boss, E., and W. S. Pegau (2001), Relationship of light scattering at an angle in the backward direction to the backscattering coefficient, *Appl. Opt.*, *40*(30), 5503–5507.
- Chelton, D. B., M. G. Schlax, R. M. Samelson, and R. A. de Szoeke (2007), Global observations of large oceanic eddies, *Geophys. Res. Lett.*, *34*, L15606, doi:10.1029/2007GL030812.
- Chelton, D. B., P. Gaube, M. G. Schlax, J. J. Early, and R. M. Samelson (2011a), The influence of nonlinear mesoscale eddies on near-surface oceanic chlorophyll, *Science*, *334*(6054), 328–332, doi:10.1126/science.1208897.
- Chelton, D. B., M. G. Schlax, and R. M. Samelson (2011b), Global observations of nonlinear mesoscale eddies, *Progr. Oceanogr.*, *91*(2), 167–216, doi:10.1016/j.pocean.2011.01.002.
- Chenillat, F., P. J. S. Franks, P. Rivière, X. Capet, N. Grima, and B. Blanke (2015), Plankton dynamics in a cyclonic eddy in the Southern California Current System, *J. Geophys. Res. Oceans*, *120*, 5566–5588, doi:10.1002/2015JC010826.
- Chisholm, S. W. (1992), Phytoplankton size, in *Primary Productivity and Biogeochemical Cycles in the Sea*, pp. 213–237, Springer, New York.
- de Boyer Montégut, C., G. Madec, A. S. Fischer, A. Lazar, and D. Ludicone (2004), Mixed layer depth over the global ocean: An examination of profile data and a profile-based climatology, *J. Geophys. Res.*, *109*, C12003, doi:10.1029/2004JC002378.
- Dubinsky, Z., and N. Stambler (2009), Photoacclimation processes in phytoplankton: Mechanisms, consequences, and applications, *Aquat. Microb. Ecol.*, *56*(2–3), 163–176.
- Dufois, F., N. J. Hardman-Mountford, J. Greenwood, A. J. Richardson, M. Feng, S. Herbette, and R. Matear (2014), Impact of eddies on surface chlorophyll in the South Indian Ocean, *J. Geophys. Res. Oceans*, *119*, 8061–8077, doi:10.1002/2014JC010164.
- Dufois, F., N. J. Hardman-Mountford, J. Greenwood, A. J. Richardson, M. Feng, and R. Matear (2016), Anticyclonic eddies are more productive than cyclonic eddies in subtropical gyres because of winter mixing, *Sci. Adv.*, *2*, e1600282, doi:10.1126/sciadv.1600282.
- Falkowski, P. G., D. Ziemann, Z. Kolber, and P. K. Bienfang (1991), Role of eddy pumping in enhancing primary production in the ocean, *Nature*, *352*, 55–58.
- Feng, M., D. Slawinski, L. E. Beckley, and J. K. Keesing (2010), Retention and dispersal of shelf waters influenced by interactions of ocean boundary current and coastal geography, *Mar. Freshwater Res.*, *61*(11), 1259–1267, doi:10.1071/MF09275.
- Feng, M., F. Colberg, D. Slawinski, O. Berry, and R. Babcock (2016), Ocean circulation drives heterogeneous recruitments and connectivity among coral populations on the North West Shelf of Australia, *J. Mar. Syst.*, *164*, 1–12, doi:10.1016/j.jmarsys.2016.08.001.
- Gaube, P., D. B. Chelton, P. G. Strutton, and M. J. Behrenfeld (2013), Satellite observations of chlorophyll, phytoplankton biomass, and Ekman pumping in nonlinear mesoscale eddies, *J. Geophys. Res. Oceans*, *118*, 1–22, doi:10.1002/2013JC009027.
- Gaube, P., D. J. McGillicuddy, D. B. Chelton, M. J. Behrenfeld, and P. G. Strutton (2014), Regional variations in the influence of mesoscale eddies on near-surface chlorophyll, *J. Geophys. Res. Oceans*, *119*, 8195–8220, doi:10.1002/2014JC010111.
- Grasshoff, K., K. Kremling, and M. Ehrhardt (2009), *Methods of Seawater Analysis*, John Wiley, Chichester, U. K.
- Halo, I., B. Backeberg, P. Penven, I. Ansrorge, C. Reason, and J. Ullgren (2014), Eddy properties in the Mozambique Channel: A comparison between observations and two numerical ocean circulation models, *Deep Sea Res., Part II*, *100*, 38–53.
- Huisman, J., N. N. P. Thi, D. M. Karl, and B. Sommeijer (2006), Reduced mixing generates oscillations and chaos in the oceanic deep chlorophyll maximum, *Nature*, *439*(7074), 322–325.
- Isern-Fontanet, J., E. García-Ladona, and J. Font (2006), Vortices of the Mediterranean Sea: An altimetric perspective, *J. Phys. Oceanogr.*, *36*(1), 87–103.
- Kalnay, E., M. Kanamitsu, R. Kistler, W. Collins, D. Deaven, L. Gandin, M. Iredell, S. Saha, G. White, and J. Woollen (1996), The NCEP/NCAR 40-year reanalysis project, *Bull. Am. Meteorol. Soc.*, *77*(3), 437–471.
- Klein, P., and G. Lapeyre (2009), The oceanic vertical pump induced by mesoscale and submesoscale turbulence, *Annu. Rev. Mar. Sci.*, *1*, 351–375, doi:10.1146/annurev.marine.010908.163704.
- Kouketsu, S., H. Tomita, E. Oka, S. Hosoda, T. Kobayashi, and K. Sato (2012), The role of meso-scale eddies in mixed layer deepening and mode water formation in the western North Pacific, *J. Oceanogr.*, *68*(1), 63–77, doi:10.1007/s10872-011-0049-9.
- Lignell, R., A. Heiskanen, H. Kuosa, K. Gundersen, P. Kuuppo-Leinikki, R. Pajuniemi, and A. Uitto (1993), Fate of a phytoplankton spring bloom: Sedimentation and carbon flow in the planktonic food web in the northern Baltic, *Mar. Ecol. Progr. Ser.*, *94*, 239–239.
- McGillicuddy, D. J. (2016), Mechanisms of physical-biological interaction at the oceanic mesoscale, *Annu. Rev. Mar. Sci.*, *8*, 13.11–13.36.
- McGillicuddy, D. J., et al. (2007), Eddy/wind interactions stimulate extraordinary mid-ocean plankton blooms, *Science*, *316*(5827), 1021–1026, doi:10.1126/science.1136256.
- McGillicuddy, D., A. Robinson, D. Siegel, H. Jannasch, R. Johnson, T. Dickey, J. McNeil, A. Michaels, and A. Knap (1998), Influence of mesoscale eddies on new production in the Sargasso Sea, *Nature*, *394*(6690), 263–266.
- Mignot, A., H. Claustre, J. Uitz, A. Poteau, F. D'Ortenzio, and X. Xing (2014), Understanding the seasonal dynamics of phytoplankton biomass and the deep chlorophyll maximum in oligotrophic environments: A Bio-Argo float investigation, *Global Biogeochem. Cycles*, *28*, 856–876, doi:10.1002/2013GB004781.
- Okubo, A. (1970), Horizontal dispersion of floatable particles in the vicinity of velocity singularities such as convergences, paper presented at Deep Sea Res. and Oceanogr. Abstr., Elsevier.
- Park, Y.-H., J.-H. Lee, I. Durand, and C.-S. Hong (2014), Validation of Thorpe-scale-derived vertical diffusivities against microstructure measurements in the Kerguelen region, *Biogeosciences*, *11*(23), 6927–6937.
- Pookkandy, B., D. Dommenges, N. Klingaman, S. Wales, C. Chung, C. Frauen, and H. Wolff (2016), The role of local atmospheric forcing on the modulation of the ocean mixed layer depth in reanalyses and a coupled single column ocean model, *Clim. Dyn.*, *47*(9–10), 2991–3010.
- Prézelin, B. B., M. M. Tilzer, O. Schofield, and C. Haese (1991), The control of the production process of phytoplankton by the physical structure of the aquatic environment with special reference to its optical properties, *Aquatic Sci.*, *53*(2), 136–186, doi:10.1007/bf00877058.
- Schlitzer, R. (2000), Electronic atlas of WOCE hydrographic and tracer data now available, *Eos Trans. AGU*, *81*(5), 45–45, doi:10.1029/00EO00028.
- Sorokin, Y. I. (1977), The heterotrophic phase of plankton succession in the Japan Sea, *Mar. Biol.*, *41*(2), 107–117.
- Stramma, L., H. Bange, R. Czeschel, A. Lorenz, and M. Frank (2013), On the role of mesoscale eddies for the biological productivity and biogeochemistry in the eastern tropical Pacific Ocean off Peru, *Biogeosci. Discuss.*, *10*(6), 9179–9211.
- Stramski, D., and D. A. Kiefer (1991), Light scattering by microorganisms in the open ocean, *Progr. Oceanogr.*, *28*(4), 343–383, doi:10.1016/0079-6611(91)90032-H.
- Talley, L. D., and M. O. Baringer (1997), Preliminary results from WOCE hydrographic sections at 80 E and 32 S in the central Indian Ocean, *Geophys. Res. Lett.*, *24*, 2789–2792, doi:10.1029/97GL02657.
- Thorpe, S. (1977), Turbulence and mixing in a Scottish loch, *Philos. Trans. R. Soc. London A*, *286*(1334), 125–181.
- Weiss, J. (1991), The dynamics of enstrophy transfer in two-dimensional hydrodynamics, *Phys. D: Nonlinear Phenomena*, *48*(2–3), 273–294.

- Westberry, T. K., G. Dall'Olmo, E. Boss, M. J. Behrenfeld, and T. Moutin (2010), Coherence of particulate beam attenuation and backscattering coefficients in diverse open ocean environments, *Opt. Express*, *18*(15), 15,419–15,425.
- Zhang, X., L. Hu, and M.-X. He (2009), Scattering by pure seawater: Effect of salinity, *Opt. Express*, *17*(7), 5698–5710.